EEGs

EEG Research

Stephen Junha Chang

Cal Poly Pomona
Computer Science
2023-2024

Contents

Abstract

This paper is a culmination of an exploration into EEGs and, by extension, their use in Affective Computing. This paper was generously supported by the PolySec Lab and advised by Professor Mohammad Husain. The aim is to deeply and broadly examine the field of EEG based imaging systems, their evolution, theory, and concerns, as well as to present a novel system of individualized sentiment analysis for interpreting EEG signals for near real-time use cases in AR and VR applications.

1 A Review of Literature

1.1 Neural activity

Neural activity – the way we measure it and the way we interpret it, are a product of the bio-electrical activity that is being observed. These electrical impulses are driven by an intricate network of biological capacitors. These networks perform complex calculations, building the biological computer that drives our senses for which builds our experience of a conscious experience. Reading these senses allow us to take a peak into the complexity that drives cognition, and perhaps how to interpret and even recreate it.

The signals collected by the electroencephalogram measure the aftermath of a biological process [5]. These signals underlie innate electrical activity described by the capacitive nature of neurons [22].

The neuron is made up of several components including the cell body (soma), dendrites, axon, axon terminals, myelin sheath, nodes of Ranvier, and synapse. Each component has functions which include the stage of capacitive storage of resting charge known as the resting potential. During this resting stage, neurons release electrical charge in response to stimulation released by a rapid change in membrane potential (also known as depolarization). After a depolarization event, re-polarization or hyper-polarization takes place to restore the charge back to a state of resting potential [7]. The propagation of these depolarization events is transmitted through the nearby connecting cellular structures of each neuron's dendrites and axon terminals of the subsequent connected neuron. This depolarization event is the function which we measure with

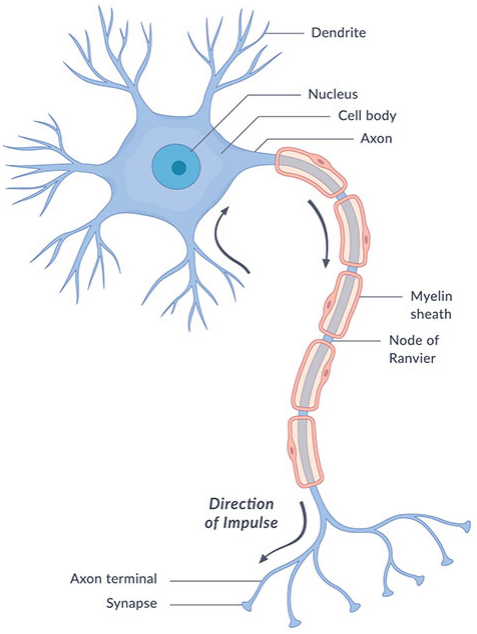

Figure 1: A Neuron [22]

EEG [21].

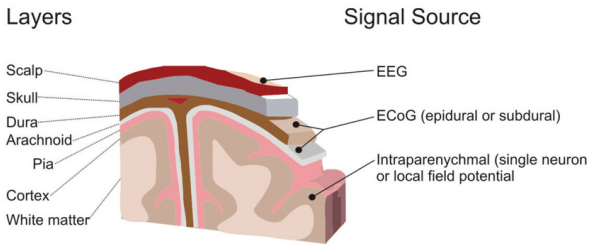

Figure 2: Layers of the Brain [5]

The measurement of the electrical activity induced by depolarization events is encumbered by the barrier between the measured neuron and the electrode. The barriers between the skin and subsequent anatomy provide a difficult lens of observation. While intracranial techniques are favored for high-resolution observation, the invasive inconvenience of surgical procedures hinders the mass adoption of the technology.

1.2 EEG

EEG – electroencephalograms, are devices that amplify neural electrical activity into interpretable or observable measures. First invented by Hans Berger in 1924, the device has been used mostly in medical applications including tumor detection, neurodegenerative diseases, stroke, sleep conditions, Creutzfeldt-Jakob disease, as well as a measure of neural activity in determining cognitive death. [31] Further explorations into the observable "rhythmic" activities have resulted in surprising clarity of state information, source activity, and correlation. [20]

1.2.1 Applications

A few interesting applications to explore are in the domain of use as an input device, as an authentication method, as a measure of stimuli, and as a cognitive interface.

As an Input Device – EEGs have been applied in gaze estimation, intent classification, and content classification. Gaze estimation has shown promising results of around $0.1707 \pm 0.011°$ in accuracy. [34] Intent classification has been fruitful in row-column selection in alphabet arrays and other selection-based applications. Variable dimensionality has mostly measured band power to variably controlled devices such as dials. [15]

As an Authentication method – there have been explorations into "thinking passwords". Unfortunately, the proposed methods to achieve this "thought to word" algorithm have not progressed further due to inherently low accuracy. [29] However, an alternative authentication method which aims to be used as a two-factor authentication method by identifying users by the physiological response to audio or visual stimuli has proven much more fruitful. [8]

Stimuli – Studies into video as a lens of decoding visual or auditory stimuli have been few and far between due to the spatial resolution and noise of measurements. [6] It has been suggested visual stimuli may require per-neuron measurements to yield any results that can recreate or estimate the subject's thought. However, low-level classification algorithms for identifying said stimuli from a set of known sources have yielded promising results. [35] The use of transformers in conjunction with brain signals for image generation has also been a recent development but has varying results in terms of efficacy and continuity of generated images.

1.2.2 Data Acquisition

The acquisition of EEG signals has evolved since its inception; however, they follow three general steps: electrode contact, amplification, then digitization. Studies have used anywhere from 8 to upwards of 250 electrodes or even high-density specialized electrodes aimed at increasing spatial resolution. The quality of raw EEG data is usually determined by three factors:

- **Spatial Resolution**: Determined by the number of electrodes.
- **Sampling Rate**: Determined by the sampling rate of the ADC (Analog to Digital Converters).
- **Impedance**: Determined by the electrode type, hardware implementation, and chosen amplification method.
- **Noise To Signal**: Determined by the electrical soundness of the EEG setup.

Electrodes – the segment of the EEG which interface between the surface of the skin and the amplification stage are generally in the following categories:

- **Cup Electrodes**: Generally require liquid conductive paste and are taped onto the head.
- **Comb Electrodes**: Generally spiked and penetrate the hair but have high impedance due to the variable contact between the spikes and the skin.
- **Polymer Electrodes**: An electrolyte-plated polymer foam which allows for dry readings with more surface area, thus reducing impedance.
- **Capacitive Electrodes**: A non-contact electrode that utilizes active electrode points to amplify the electrical wave interpolation caused by neural activity.

Amplification – The stage to allow for the signals to be observable by a ADC (analog to digital converter) can be achieved by low-noise amplifiers. There are two general methods of amplification:

- **Active**: Uses amplification on the electrode itself instead of a centralized amplification stage. This allows the secondary amplification stage to prevent amplifying noise collected in the wiring from the electrode to the amplifier circuit.
- **Passive**: Uses an electrode connected to a centralized electronic amplification device. This amplification device has a process of RF filtering, which is then digitized into data through said centralized amplification stage.

Each method has its advantages and pitfalls. Between variable contact consistency, resolution, complexity, and comfort, each method can vastly impact the form and context that the EEG can be used in.

1.2.3 Filtering

In the EEG signals collected by our aforementioned collection methods, we can observe several artifacts and sources of noise that are not of interest, such as muscle artifacts (motion, muscular, ocular, and cardiac) [3] and electrical interference (power line, device, and thermal/charge) [16].

Several methods of noise removal must be undertaken, such as simple band pass filters (high-pass filters, low-pass filters, and notch filters) for electrical interference. Furthermore, more advanced methods such as Independent Component Analysis (ICA) may be used to remove muscle artifacts.

Bandpass Filtering – These methods will remove signal frequencies that are well-known sources of noise. Such frequencies are 50 Hz and 60 Hz, which can be mitigated by notch filters (50 Hz for non-US AC noise and 60 Hz for US AC) [16]. Furthermore, a low-pass of 100 Hz and high-pass of 0.5 Hz is used to isolate useful frequency ranges related to neural activity.

Hardware Filtering – Before software filtering, we can ensure a cleaner dataset through RF filters, which can act to eliminate 50 Hz and 60 Hz noise. This is usually done through a twin-T filter.

Software Filtering We use the SciPy implementation of a Butterworth filter, performing a low-pass on 60 Hz, high-pass on 0.5 Hz, and a band-stop at both 50 Hz and 60 Hz. A Butterworth filter is defined as:

$$H(s) = \frac{G}{1 + \left(\frac{s}{\omega_c}\right)^{2n}}$$

where:

- $H(s)$ is the filter's transfer function.
- G is the DC gain.
- s is the complex frequency variable in the Laplace domain.
- ω_c is the cutoff frequency.
- n is the order of the filter.

1.2.4 Artifact Filtering

Muscle artifacts are the next challenge that we face, which are characterized by "surges in high-frequency activity" [3]. These artifacts are usually mitigated by removing high kurtosis and correlation in components returned by Independent Component Analysis (ICA) [4].

Independent Component Analysis – ICA is a method of linearly separating n mixed sources into n independent components. In the context of EEG signal filtering, we will use FastICA, which is a process that can be generalized into three distinct steps of data centering, data whitening, and data transformation. In ICA, we aim for the sources (the individual channels) of the mixed matrix to be independent and non-Gaussian.

Centering For n observed signals $X = [x_1, x_2, \ldots, x_i]$, where x_i is a vector of length κ (the channel count), we center the data:

$$X_{\text{centered}} = X - \text{mean}(X)$$

Subtracting the column values by the mean of the column.

Whitening For X_{centered}, we perform an eigenvalue decomposition on the covariance matrix:

$$X_{\text{centered}} = EDE^T$$

where D is a diagonal matrix whose elements are eigenvalues of C, and E is a matrix with its columns being corresponding eigenvectors.

Transform We find the whitening transformation W using the eigenvectors and eigenvalues as follows:

$$W = D^{\frac{-1}{2}} E^T$$

where $D^{-\frac{1}{2}}$ is the diagonal matrix with the inverse square roots of eigenvalues. Then, the whitened data Y is found by applying the transformation to the centered data:

$$Y = WX_{\text{centered}}$$

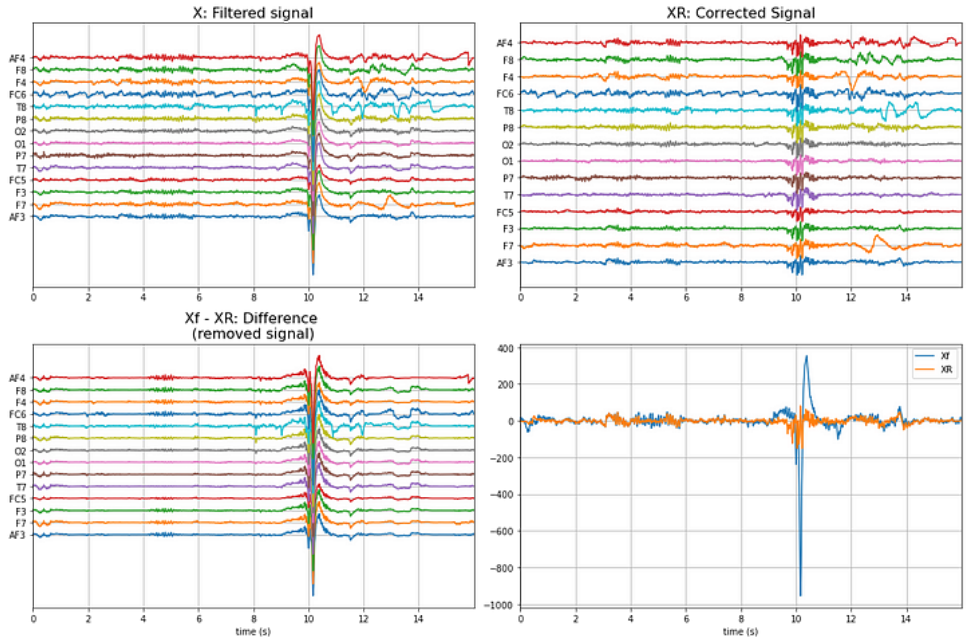

Figure 3: Comparison of Independent Component Analysis (ICA) results [4].

Furthermore, we can filter out individual components with high kurtosis and correlation, remixing the signals with the removed component for each channel.

Empirical Mode Decomposition(EMD) – is a signal processing technique that decomposes a signal into individual Intrinsic Mode Functions (IMFs) in the time domain. An IMF is defined as a function with only one extreme between zero crossings and has a mean value of zero.

The steps for EMD are:

1. Use cubic spline interpolation method for $e_{\max}$ and $e_{\min}$ (envelopes of maxima and minima).
2. Calculate mean $m(t) = \frac{e_{\max}+e_{\min}}{2}$.
3. Calculate the difference $d(t) = x(t) - m(t)$.
4. Repeat until $d(t)$ satisfies the definition of an IMF.

With the prevalence of different methods of classifying the aforementioned features into sentiment, we analyze a few different comparative studies between the different classification methods and the features used based on the contextual model accuracy.

1.2.5 Features

Approximate Entropy If we consider an array of data of length m and tolerance level r (which represents a fraction of the standard deviation of the EEG signals), and X_i is an array $[x_i(1), x_i(2), \ldots, x_i(m)]$ in which $x_i(k)$ represents the EEG amplitude at $i + k - 1$.

If we compute the Euclidean distance between X_i and X_j where i and j range from 1 to $N - m + 1$, then compute the number of pairs where the distance is less than or equal to r, denoted $C_m(r)$, we then know that the approximate entropy is:

$$\mathrm{ApEn}(m, r) = \ln(C_m(r)) - \ln(C_{m+1}(r))$$

Wavelet Entropy – We can also compute the wavelet entropy [27]. We apply a wavelet transform:

$$W(a, b) = \int_{-\infty}^{\infty} x(t)\psi_{a,b}(t)\, dt$$

Then extract the wavelet coefficient:

$$c_{j,k} = \langle x(t), \psi_{j,k}(t) \rangle$$

Then calculate the (Shannon) entropy with:

$$H(X) = -\sum_{i=1}^{n} p_i \log_2(p_i), \quad p_i = \frac{|c_i|^2}{\sum_{i=1}^{n} |c_i|^2}$$

Fast Fourier Transform – $F(\omega) = \int_{-\infty}^{\infty} f(t)e^{-i\omega t}\, dt$
Fast Fourier Transform is a method of Fourier transform which transforms a time domain to a frequency domain. It is represented by:

Where $e^{i\omega t}$ is a complex exponential function in which i is the imaginary unit and ω is the frequency parameter. The integral computes the frequency components of $f(t)$.

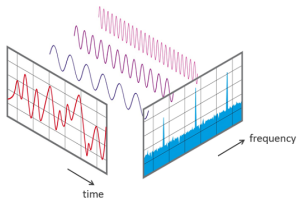

Figure 4: Fast Fourier Transform (FFT)

Band Power We can further dimensionally reduce the known band power by grouping the signal bands into known associated Beta, Alpha, Theta, and Delta frequency ranges, finding the power of each

band for a given time frame [14]. EEG signals have classically been classified into five band classifications: Alpha (α), Theta (θ), Delta (δ), Beta (β), Gamma (γ).

Wave	**Frequency Range (Hz)**	**State**
Delta	0.5–4	Deep Sleep
Theta	4–8	Drowsiness, Dreams, Creativity
Alpha	8–15	Calmness, Relaxation, Abstract Thinking
Beta	16–31	Focus, Alertness
Gamma	32+	Perception, Short-term Memory

Table 1: Frequency Bands [20]

Higuchi's Fractal Dimension Higuchi's fractal dimension [33] is an estimation of the fractal dimension of a signal, measuring the complexity of a pattern. It can provide information on the dynamics and complexity of a given signal, characterizing abnormalities and non-linear dynamics.

Given a time series, it divides the segments into varied lengths. For each segment of length k, the average length of the curve by connecting the m-th point of $[1..k]$ results in a set of curve lengths for given segments. When averaging the curve lengths, the fractal dimension is found by:

$$L_m(k) = \frac{\left\{\sum_{i=1}^{\left\lfloor \frac{N-m}{k} \right\rfloor} |x(m+ik) - x(m+(i-1)k)| \frac{N-1}{\left\lfloor \frac{N-m}{k} \right\rfloor} k\right\}}{\left\lfloor \frac{N-1}{\left\lfloor \frac{N-m}{k} \right\rfloor} k \right\rfloor}$$

1.2.6 Classification

Classification is a extremely wide-ranging subject area that has been extensively explored for each of the different applications and processing methods. Each has strengths and weaknesses, with a few of the most prevalent being listed below.

Support Vector Machine (SVM) – Support Vector Machines allow for an intersection between classification and regression. It generally functions by optimizing an n-dimensional hyperplane that effectively splits the data between categories. It is effective for dimensionally large input features [10] such as EEG features.

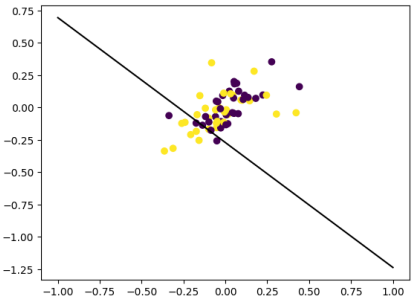

Figure 5: Support Vector Machine (SVM)

SVM has been a popular method of classification, with positive/negative classifica-

tion topping around 91.77% in combina-
tion with LDA method for binary classification [25]. Furthermore, it is the most popular method, accounting for 70% of EEG classification studies [25].

The general decision function is as follows:

$$f(x) = \text{sign}(w \cdot x + b)$$

where:

- w is the weight vector perpendicular to the hyperplane.
- x is the input feature vector.
- b is the bias term.

To maximize margins between support vectors, it applies an objective function:

$$\min_{w,b} \frac{1}{2}||w||^2$$

constrained by:

$$y_i(w \cdot x_i + b) \geq 1$$

Soft Margins Soft margins can be applied by the objective function:

$$\min_{w,b} \frac{1}{2}||w||^2 + C\sum_{i=1}^{n} \xi_i$$

constrained by:

$$y_i(w \cdot x_i + b) \geq 1 - \xi_i$$

$$\xi_i \geq 0$$

We can also map the features into a higher dimension by using the Kernel trick:

$$f(x) = \text{sign}\left(\sum_{i=1}^{n} \alpha_i y_i K(x_i, x) + b\right)$$

where α_i are the Lagrange multipliers of the kernel function $K(x_i, x)$.

Recursive Neural Network (RNN) – Recursive Neural Networks function similarly to normal forward-feeding neural networks. However, there is a recursive feed of the hidden state to the previous node, allowing the network to capture temporal dynamics.

Convolutional Neural Network (CNN) – Convolutional Neural Networks are feed-forward networks that use convolution layers to effectively extract features that are more indicative of certain characteristics. Convolution layers are field-region varied learning filters with parameter sharing between inputs that produce a two-dimensional feature map.

CNNs have been an interesting approach as they can learn from local receptive fields, which allows for effective learning from overlapping input regions. This has given hope for the use of CNNs in the highly dynamic and dimensionally complex feature set of EEG signals [36].

In a fully connected layer in a neural network:

$$y_{mn} = f(XW + b)$$

where:

- $Y_{m,n}$ is the output of the layer at (m, n).
- X represents the input matrix.
- W is the weight matrix in which w_{ij} represents the weight of the i-th input feature and j-th neuron.
- b is the bias vector b_j of the j-th neuron.

The function applied is:

$$y_{mn} = f\left(\sum_{j=0}^{J-1}\sum_{i=0}^{I-1} x_{m+i,n+j}w_{ij} + b\right)$$

where f is the activation function applied to $x_{m+i,n+j}$ input values, with w_{ij} weights of the input values, and b the bias term.

Random Forest – Random Forest is essentially a collection of decision trees, where each tree outputs a class prediction and the class with the most votes becomes the model's prediction. It is an ensemble learning method that is effective for handling non-linear data but may struggle with high-dimensional, noisy data.

Review – The overwhelming quantity of different and custom learning algorithms provides an interesting point of comparative analysis for the effectiveness of feature-classification pairs. However, the exploration of deep neural networks may provide a path to more complex analysis of the hidden nature of neural EEG signals.

1.3 Affective Computing

Affective Computing is the study and development of systems that recognize, interpret, and process human emotions to improve user interaction. EEG may be an important avenue in this field, especially in its potential for providing real-time insights into neural activity correlated with emotional states.

2 Initial Thoughts

From the literature, we observe the litany of approaches we could take for the numerous possible applications. I felt it would be important to define the possible limitations of the applciations of EEG, and explore whether or not certain claims could be possibly innovated on.

2.1 Resolution

Our analysis progresses from examining the fundamental physics of neural electrical properties to interpreting the data provided by electroencephalography (EEG). Understanding the propagation of neural signals through brain tissues is crucial for developing technologies that interpret EEG signals for applications like emotion recognition.

Neurons in the cognitive areas of the brain are approximately 680×10^{-6} meters long [13]. At rest, neurons maintain a resting potential of -70 millivolts (mV). When a neuron is stimulated, reaching a threshold potential of -55 mV, it undergoes an action potential where the membrane potential rapidly spikes due to the influx of sodium ions.

Based on this, we can calculate the propagation model for the neural impulse signal. The electrical signal generated by neural activity must propagate through several layers before it can be collected by the EEG. The layers, along with their electrical properties, are shown in Table 2.

Tissue	**Resistivity** ($\Omega\,\mathrm{m}$)	**Conductivity** ($\mathrm{S\,m^{-1}}$)	**Density** ($\mathrm{kg\,m^{-3}}$)
Brain	5	0.2381	1030
CSF	0.65	1.538	1060
Dura (Soft Tissue)	5.76	0.17361	1050
Hard Bone	160	0.00625	1850
Skin	2.3	0.43478	1100

Table 2: Electrical properties of various brain and tissue layers relevant to EEG signal propagation [26, 28]

To understand how neural activity attenuate as they propagate through different tissue layers to reach EEG electrodes, we calculate the impedance of each layer. This helps estimate the signal strength at the scalp and the number of neurons required to produce a detectable EEG signal.

Best Case – For low-frequency signals typical of EEG (less than 100 Hz), capacitive effects are often negligible compared to resistive effects. Using Ohm's Law $V = I \times Z$, we calculate the minimum current I_{scalp} required at the scalp:

$$I_{\text{scalp}} = \frac{V_{\text{EEG}}}{Z_{\text{total}}} = \frac{1 \times 10^{-6}\,\text{V}}{1.01301\,\Omega} \approx 9.87 \times 10^{-7}\,\text{A}$$

So, approximately $0.987\,\mu\text{A}$ of current is required at the scalp.

The signal attenuates significantly as it passes through tissue layers. Empirical studies suggest that only about 0.1% (attenuation factor $A = 0.001$) of the cortical current reaches the scalp.

Considering an attenuation:

$I_{\text{cortex}} = \frac{I_{\text{scalp}}}{A} = \frac{9.87 \times 10^{-7}\,\text{A}}{0.001} = 9.87 \times 10^{-4}\,\text{A}$

So, approximately $987\,\mu\text{A}$ of current is required at the cortical level.

Estimate the current generated by a single neuron:

$C_{membrane}\ 1\,\mu\text{F/cm}^2\ A_{surface}\ (A_{\text{neuron}})$

Assuming a cylindrical neuron:

$L = 680\,\mu\text{m} = 6.8 \times 10^{-2}\,\text{cm}$

$D = 10\,\mu\text{m} = 1 \times 10^{-3}\,\text{cm}$

$A_{\text{neuron}} = \pi DL = \pi \times (1 \times 10^{-3}\,\text{cm}) \times (6.8 \times 10^{-2}\,\text{cm}) \approx 2.136 \times 10^{-4}\,\text{cm}^2$

$C_{\text{neuron}} = (1\,\mu\text{F/cm}^2) \times (2.136 \times 10^{-4}\,\text{cm}^2) = 2.136 \times 10^{-4}\,\mu\text{F}$

Membrane potential change (ΔV) is approximately 100 mV:

$Q = C_{\text{neuron}} \times \Delta V = (2.136 \times 10^{-4}\,\mu\text{F}) \times (100\,\text{mV}) = 21.36\,\text{pC}$

If the action potential lasts about $t = 1\,\text{ms}$

$I_{\text{neuron}} = \frac{Q}{t} = \frac{21.36 \times 10^{-12}\,\text{C}}{1 \times 10^{-3}\,\text{s}} = 21.36 \times 10^{-9}\,\text{A} = 21.36\,\text{nA}$

So, each neuron contributes approximately 21 nA of current during an action potential.

Calculate the number of neurons N:

$N = \frac{I_{\text{cortex}}}{I_{\text{neuron}}} = \frac{9.87 \times 10^{-4}\,\text{A}}{21.36 \times 10^{-9}\,\text{A}} \approx 46,200$

Given a signal recovery of 1 percent: $N_{\text{adjusted}} = \frac{N}{S} = \frac{46{,}200}{0.01} = 4,620,000$

So, approximately $4,620,000$ neurons need to fire synchronously.

Dipole Calculation – With a secondary calculation of dipole moment approach which considers the electric potential generated by neural activity in a volume conductor, we can get a theoretical range of the characteristics of observable neural activity.

The dipole moment p_{neuron} of a single neuron is calculated as $p_{\text{neuron}} = Q \cdot d$ where: $Q = 1 \times 10^{-12}\,\text{C}$ is the charge separation during an action potential and $d = 680 \times 10^{-6}\,\text{m}$ is the length of the neuron. Calculating: $p_{\text{neuron}} = (1 \times 10^{-12}\,\text{C})(680 \times 10^{-6}\,\text{m}) = 6.8 \times 10^{-16}\,\text{C}\cdot\text{m}$

The potential V at a distance r from a dipole p_{total} in a homogeneous volume conductor is given by: $V = \frac{p_{\text{total}}}{4\pi\sigma r^2}$ Solving for p_{total} where $V = 1 \times 10^{-6}\,\text{V}$ (detectable EEG signal), $\sigma = 0.33\,\text{S/m}$ (average conductivity of head tissues), $r = 0.08\,\text{m}$ (distance from cortical neurons to scalp). $p_{\text{total}} = 4\pi\sigma V r^2$ $p_{\text{total}} = 4\pi(0.33)(1 \times 10^{-6})(0.08)^2 = 2.65 \times 10^{-8}\,\text{C}\cdot\text{m}$

Calculating the number of neurons N required: $N = \frac{p_{\text{total}}}{p_{\text{neuron}}} = \frac{2.65 \times 10^{-8}}{6.8 \times 10^{-16}} \approx 3.9 \times 10^{7}$ Approximately 39 million synchronously active neurons are needed to produce a $1\,\mu\text{V}$ EEG signal at the scalp.

Discussion – 39 million synchronously active neurons calculated as necessary to achieve a theoretical $5 - 10$ percent signal recovery would limit us to a maximum spatial resolution of approximately $2 - 5cm$ which is similar to the observed limitations of 6-9cm [2]. This is because identifying the average signal location depends on concurrent firing of neuron clusters, but it does not allow us to trace the signal pathway.

2.2 Limitations

Limitations in specific cognitive stimuli – Intuitively, it is then a difficult process to trace, let alone interpret the neural density to reconstruct visual stimuli given mammals such as the Etruscan shrew has neuron counts of around 1 million per hemisphere [19] which facilitates senses such as touch, smell, and vision pointing towards a

factor of spatial resolution required to process visual stimuli and perhaps multiple high resolution imaging of how the brain is interpreting the visual stimuli in the estimated 4-6 billion neurons in the human visual cortex [32]. Perhaps the type of imaging required to process human visual stimuli may be exemplified by Neuralink's recent successes in using intra-cranial EEGs as a high quality input device where "System A can record 1,344 of 1,536 channels simultaneously, with the exact channel configuration arbitrarily adjustable during recording; System B can record from all 3,072 channels simultaneously" [18]. These systems achieve this using a needle density of 10.83 needles per mm^2, enabling movement resolution approximating a 100×100 grid.

Sentiment Analysis However, while it may not be possible to interpret specific cognitive functions, the use of EEGs in sentiment analysis proposes that perhaps we can find generalized cognitive trends in certain activity types which may indicate a certain emotion or reactions. As we look into this field, we come to two important questions:

1. How do we quantify emotions
2. How do we interpret emotions

These questions are often reduced to a scale of valence and arousal [17] which define "valence(positive/negative, pleasant/unpleasant)[and] arousal(calm/excited)" [1] as a theory of emotional measurement. However, even with a simplified model such as this, there are not many models that can consistently provide accurate readings across different datasets and individuals. This is exemplified in a much more studied field of EEG-Text where several models have been found to have "consistent performance across EEG and random inputs rais[ing] concerns about whether the models are genuinely learning text-related information from EEG data." [12] Furthermore, there is a concern raised on how laboratory environment and the five concerns in eliciting emotion "Subject elicited vs event-elicited, lab-setting vs real-world, expression vs feeling, open-recording vs hidden-recording, and emotion-purpose vs other-purpose" [24] We can also see that generalization/individualization is a issue in these studies, resulting from a 94.38-94.72 percent accuracy rate to 68.14-63.94 percent accuracy on a binary classification [11] which would imply that while there is some amount of learning present in the model, it may be external factors such as micro-muscular movements that may be the cause of the learning, not the neural activity. Further concern on the methodology of the model training and testing is exacerbated by the often lack of a code source for replication for peer review.

3 Proposed Method

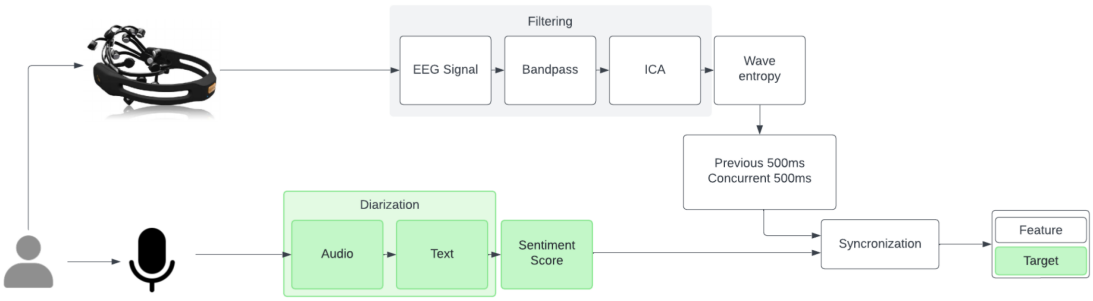

Figure 6: SVM with Soft Margins

In this paper, I propose a new EEG based sentiment analysis that would be generalizable. The major difficulty of conducting and applying EEG studies mainly lie in the labeling and collection phase. This paper aims to use a well-developed speech diarization technology as a possible means to ground EEG data for binary sentiment analysis. Oftentimes, EEG studies require participants to manually respond with their sentiment preceding the initial introduction of a stimuli. However, the sample size of this collection method is generally low and furthermore presents difficulties when attempting to create a scalable and generalizable model. Speech diarization was chosen on the basis that the participant's speech may indicate their internal preferences, allowing passive data collection without direct intervention or test against a known stimuli. We used a 14 channel EEG (EmotivEpocX) which utilizes a common-mode noise rejection system. The sampling rate is set at 256Hz. For our audio, we used a Scarlet 6i6 (1st Gen) which was connected to a XLR microphone. We collect a varied number of synchronized five second interval audio and EEG. The reason for this is to increase confidence in the spoken words transcribe in later processes. The audio is stored as a .wav file and the EEG is stored as a .csv format. The recording of the EEG is stored as a 1300 by 14 time-series array.

3.1 Hardware

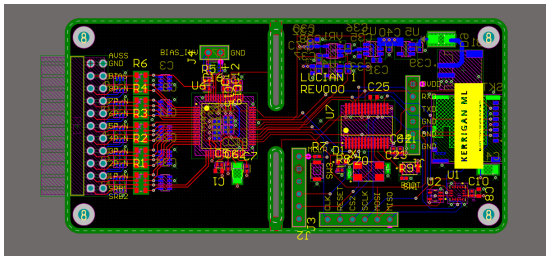

Figure 7: Version 1 with PIC32

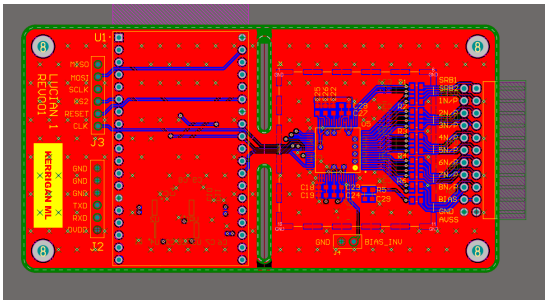

Figure 8: Version 2 with ESP32

The Amplifier For our paper, we created two custom low noise analog electrical boards. The first version used a PIC32 micro-controller with a ADS1299 8-Channel 24-Bit Analog-to-Digital Converter while the second version used a much more accessible ESP32 micro-controller with port interfaces with the same ADS1299. The inspiration for this circuit mainly came from the Open-BCI circuitry. While these were promising in their predictability, we found that hand soldering caused inconsistencies in operation, leading us to use a standard 16 channel Emotiv Headset.

3.2 Filtering

ICA (Artifact Removal) Furthermore, more advanced methods such as Independent Component Analysis (ICA) was used to remove muscle artifacts based on a threshold kurtosis and correlation value.

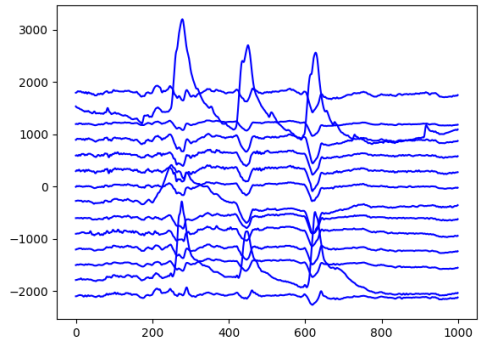

Figure 9: Raw Signal

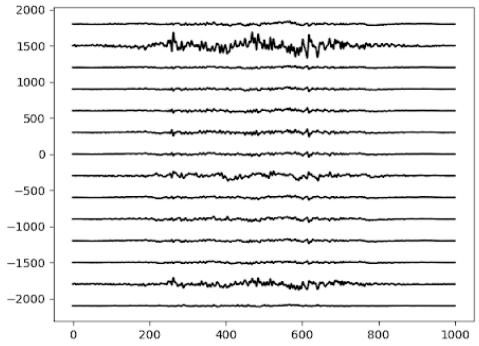

Figure 10: Signal After ICA

Band Pass Removal of well-known frequencies sources of noise. (50Hz) for non-US AC noise and (60Hz) for US AC noise with notch filter and bandpass at 0.5hz to 100hz.

3.3 Diarization and Synchronization

Using the previously created audio files, we used a Dynamic Time Warping analysis on top of the Whisper model developed by OpenAI for second-by-second timestamps per each word. The timestamps are used to find the initial point of reference and the previous and preceding 500ms appended to the EEG data.

3.4 Classification

For our initial exploration, we used wavelet entropy and approximate entropy of the previous and proceeding windowed data.

Target Word by word analysis through the Afinn library was used for sentiment analysis of the text labeled (0 and 1).

Training Support Vector Machines allows for an intersection between classification and regression. It generally functions by optimizing a n-dimensional hyperplane that effectively splits the data between categories. It is effective for dimensionally large input features such as EEG features.

3.5 Results

With a small sample size of 528 words, we can observe around 97.169 percent accuracy in binary classification between "Positive" and "Neutral". When looking at a model trained with data that is normalized for positive and negative inferences (balancing the training set), we can see that it leads to an accuracy of 71.428 percent.

3.6 Conclusion

This method of sentiment analysis seems to show promising results. It seems that further data collection would be required to validate the data in consideration of the relatively low precision for true positives. Due to the extremely low use of sentiment indicative words in normal conversation, we've found that merely 6 percent of the words could be used for positive or negative indication. Future works would normalize sample distribution for positive and non-positive training and testing sets with larger training data. An exploration of multi-class classification would be an interesting direction of this research.

References

[1] The neurobiology of emotional experience. *The Journal of Neuropsychiatry and Clinical Neurosciences*, 9(3):439–448, 1997. PMID: 9276845.

[2] F Babiloni, F Cincotti, F Carducci, PM Rossini, and C Babiloni. Spatial enhancement of eeg data by surface laplacian estimation: the use of magnetic resonance imaging-based head models. *Clinical Neurophysiology: Official Journal of the International Federation of Clinical Neurophysiology*, 112(5):724–727, May 2001.

[3] C. Brunner et al. Muscle artifacts in the eeg. *Journal of Clinical Neurophysiology*, 13(2):157–168, 1996.

[4] A. Delorme and S. Makeig. Eeglab: an open source toolbox for analysis of single-trial eeg dynamics including independent component analysis. *Journal of Neuroscience Methods*, 134(1):9–21, 2004.

[5] G. Dornhege, J. del R. Millán, T. Hinterberger, D. McFarland, and K. R. Müller, editors. *Toward Brain-Computer Interfacing*. MIT Press, 2007.

[6] Matteo Ferrante, Tommaso Boccato, Stefano Bargione, and Nicola Toschi. Decoding visual brain representations from electroencephalography through knowledge distillation and latent diffusion models. *Computers in Biology and Medicine*, 178:108701, 2024.

[7] J. Grider and K. Maloney. *Physiology, Action Potential*. StatPearls Publishing, 2023.

[8] Luis Gutierrez and Mohammad Husain. Composing an electroencephalography biometric for android os with eeg workbench. 2017.

[9] KM Heilman. The neurobiology of emotional experience. *Journal of Neuropsychiatry and Clinical Neurosciences*, 9(3):439–448, 1997.

[10] S. H. Hsu and P. H. Wang. Proliferation of machine learning in electrophysiology: applications, challenges, and future directions. *Journal of Electrocardiology*, 69:32–38, 2022.

[11] Dongmin Huang, Sentao Chen, Cheng Liu, Lin Zheng, Zhihang Tian, and Dazhi Jiang. Differences first in asymmetric brain: A bi-hemisphere discrepancy convolutional neural network for eeg emotion recognition. *Neurocomputing*, 448:140–151, 2021.

[12] Hyejeong Jo, Yiqian Yang, Juhyeok Han, Yiqun Duan, Hui Xiong, and Won Hee Lee. Are eeg-to-text models working?, 2024.

[13] Eric R. Kandel, James H. Schwartz, and Thomas M. Jessell. *Principles of Neural Science*. McGraw-Hill, 4th edition, 2000.

[14] L. W. Ko, R. K. Chikara, Y. K. Wang, and C. T. Lin. Spectral entropy analysis on eeg signals during perception of emotional audiovisual contents. *Frontiers in Neurorobotics*, 14:617531, 2021.

[15] Dean J Krusienski and Jerry J Shih. Control of a visual keyboard using an electrocorticographic brain-computer interface. *Neurorehabilitation and Neural Repair*, 25(4):323–331, May 2011. Epub 2010 Oct 4.

[16] S. Leske and S. S. Dalal. Reducing power line noise in eeg and meg data via spectrum interpolation. *NeuroImage*, 189:763–776, 2019.

[17] Malek Mneimne, Alice S. Powers, Kate E. Walton, David S. Kosson, Samantha Fonda, and Jessica Simonetti. Emotional valence and arousal effects on memory and hemispheric asymmetries. *Brain and Cognition*, 74(1):10–17, 2010.

[18] Elon Musk. An integrated brain-machine interface platform with thousands of channels. *J Med Internet Res*, 21(10):e16194, Oct 2019.

[19] RK Naumann, F Anjum, C Roth-Alpermann, and M Brecht. Cytoarchitecture, areas, and neuron numbers of the etruscan shrew cortex. *Journal of Comparative Neurology*, 520(11):2512–2530, Aug 2012.

[20] E. Niedermeyer and F. L. da Silva. *Electroencephalography: Basic Principles, Clinical Applications, and Related Fields.* Lippincott Williams & Wilkins, 2005.

[21] G. D. Norata et al. The neuron: A brief introduction to structure and function. *Neuron*, 110(1):1–4, 2023.

[22] National Institutes of Health. What are neurons, and what do they do? Technical report, NIH Publication No. 18-NS-5180, 2018.

[23] B. Pakkenberg and H.J.G. Gundersen. Neocortical neuron number in humans: effect of sex and age. *Journal of Comparative Neurology*, 384(2):312–320, 1997.

[24] R.W. Picard, E. Vyzas, and J. Healey. Toward machine emotional intelligence: analysis of affective physiological state. *IEEE Transactions on Pattern Analysis and Machine Intelligence*, 23(10):1175–1191, 2001.

[25] M. M. Rahman and A. Sarkar. Recognition of emotion by eeg signal analysis: a comprehensive survey. *IEEE Transactions on Affective Computing*, 2021.

[26] Ceon Ramon, Jens Haueisen, and Paul Schimpf. Influence of head models on neuromagnetic fields and inverse source localizations. *Biomedical Engineering Online*, 5:55, February 2006.

[27] O. A. Rosso and A. Mairal. Characterization of time dynamical evolution of electroencephalographic records. *Physica A: Statistical Mechanics and its Applications*, 312(3-4):469–504, 2007.

[28] A.I. Sabbah, Nihad Dib, and M. Al-Nimr. Evaluation of specific absorption rate and temperature elevation in a multi-layered human head model exposed to radio frequency radiation using the finite-difference time domain method. *IET Microwaves, Antennas & Propagation*, 5:1073–1080, July 2011.

[29] Julie Thorpe, Paul Oorschot, and Anil Somayaji. Pass-thoughts: Authenticating with our minds. *IACR Cryptology ePrint Archive*, 2005:121, 01 2005.

[30] J. Urquiza, M. Rodríguez, and J.C. Corrales. Improving eeg signal analysis using independent component analysis and machine learning. *Neurocomputing*, 512:659–670, 2023.

[31] Merck Manual Professional Version. Electroencephalography (eeg). `https://www.merckmanuals.com/professional/neurologic-disorders/neurologic-tests-and-procedures/electroencephalography-eeg`. Accessed: 2024-11-16.

[32] BA Wandell, SO Dumoulin, and AA Brewer. Visual field maps in human cortex. *Neuron*, 56(2):366–383, Oct 2007.

[33] A. Wanliss and K. Showalter. Efficient estimation of the higuchi fractal dimension. *Chaos, Solitons & Fractals*, 152:111355, 2022.

[34] Nina Weng, Martyna Plomecka, Manuel Kaufmann, Ard Kastrati, Roger Wattenhofer, and Nicolas Langer. An interpretable and attention-based method for gaze estimation using electroencephalography, 2023.

[35] Ruiqi Yang and Eric Modesitt. Vit2eeg: Leveraging hybrid pretrained vision transformers for eeg data, 2023.

[36] X. Zhao et al. A multi-branch 3d convolutional neural network for eeg-based motor imagery classification. *IEEE Transactions on Neural Systems and Rehabilitation Engineering*, 26(10):2226–2235, 2018.